25th ABCM International Congress of Mechanical Engineering
October 20-25, 2019, Uberlândia, MG, Brazil

EVALUATION OF UNCERTAINTY ASSOCIATED WITH FRACTURE TOUGHNESS OF THE INCONEL 718 USING THE SNTT METHOD

Guilherme Bernardes Rodrigues
Monique Alves Franco de Moraes Freitas
Rosenda Valdés Arencibia
Henry Fong Hwang
Sinésio Domingues Franco
Universidade Federal de Uberlândia, 2121 João Naves de Ávila Avenue
guilhermebernardes@ufu.br
monique_afm@hotmail.com
rosenda.arencibia@ufu.br
henry@fau.ufu.br
sdfranco@ufu.br
Waldek Wladimir Bose Filho
Escola de Engenharia de São Carlos – USP, 400 Trabalhador São-Carlense Avenue
waldek@sc.usp.br

Abstract.
The Spiral Notch Torsion Test method, SNTT, allows the fracture toughness determination in pure torsion loading condition, using a cylindrical specimen with a helicoidal V-notch with 45° pitch angle. The objective of this work was to evaluate the uncertainty associated with the Linear-Elastic Plane-Strain Fracture Toughness (K_{IC}) value estimated from analytical models. For this purpose, the Monte Carlo method was applied, considering an Inconel 718 test specimen. It was concluded that the input variable "crack length" was the factor that showed the largest combined standard uncertainty and the average fracture toughness value ratio, 0.59 %. The uncertainty values associated with fracture toughness, when estimated analytically, were low, representing 1.1 % of the average value. This work brings the necessary traceability imposed by the ISO/IEC 17025 standard, improving the research scientific rigor and, therefore, in the publications in the area.

Keywords: *measurement uncertainty, Inconel 718, SNTT, K_{IC}.*

1. INTRODUCTION

In the last decades, fracture mechanics has proved to be a powerful tool in establishing the structural integrity of high responsibility mechanical structures and parts. Fracture toughness, which can be determined by different standards, depending on the material type or specimen geometry. For metals, it is generally defined by ASTM E740-88 (ASTM, 2001), ASTM E399-90 (ASTM, 2017) or ASTM 1820 (ASTM, 2001) and it is understood as the property that establishes the ability of the material to withstand a cracklike defect without failure. At the beginning of the 20th century, several methods that aimed to estimate this property were developed, using specimens such as the compact tension, C(T) the three-point bending, SE(B), among others, which were later standardized. However, these conventional methods, eventually present some significant limitations, especially with respect to the specimen size, which should be sufficient to ensure the plane stress state dominance at the fatigue pre-crack front (Wang et al., 2004).

As an alternative to the conventional method limitations, Wang et al. (2002) developed a method capable of estimating fracture toughness: The Spiral Notch Torsion Test - SNTT. This method allows the fracture toughness determination by applying pure torsion to cylindrical specimens with a V-notch with an angle of 60° and in a pitch angle of 45°. This pure torsion establishes a uniform equibiaxial tensile field of tension/compression, thus effectively developing a failure Mode I (aperture mode), as shown in Fig. 1. Thus, it is possible to obtain an intrinsic fracture toughness value of the tested material, eliminating the specimen dimension effect and establishing a more reliable and economical test. This test is still capable of having a consistent and stable crack propagation.

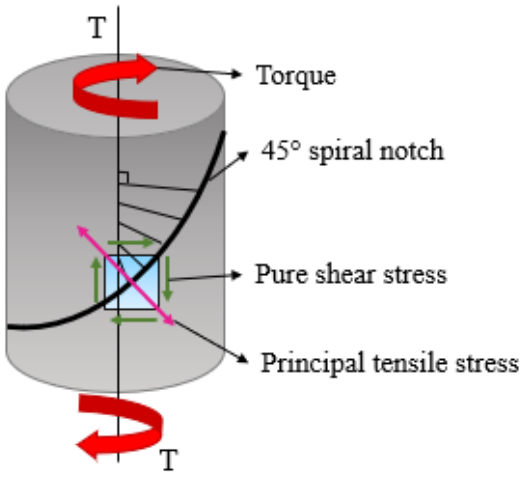

Figure 1. Schematic of SNTT theory (Adapted from WANG, 2019).

Figure 2 shows a geometric comparison between the SNTT and a C(T) specimens. The C(T) specimen has been widely used because its geometric configuration is the closest to what happens in practice with regard to the crack nucleation and propagation. Consequently, the results of C(T) tests are accepted by the academic community as those with greater reliability. Although it is the most reliable test, it has a very important simplification. Theoretical conditions are never replicated when there are free surfaces at the ends of the specimen. It is worth mentioning that the lower the specimen thickness, the greater the ends effect. This explains the limitation of conventional methods in relation to the specimen dimensions. The major problem is that the thicker the specimen, the larger all its other dimensions, consequently the greater quantity of material consumed and the larger the test system required (WANG, 2019).

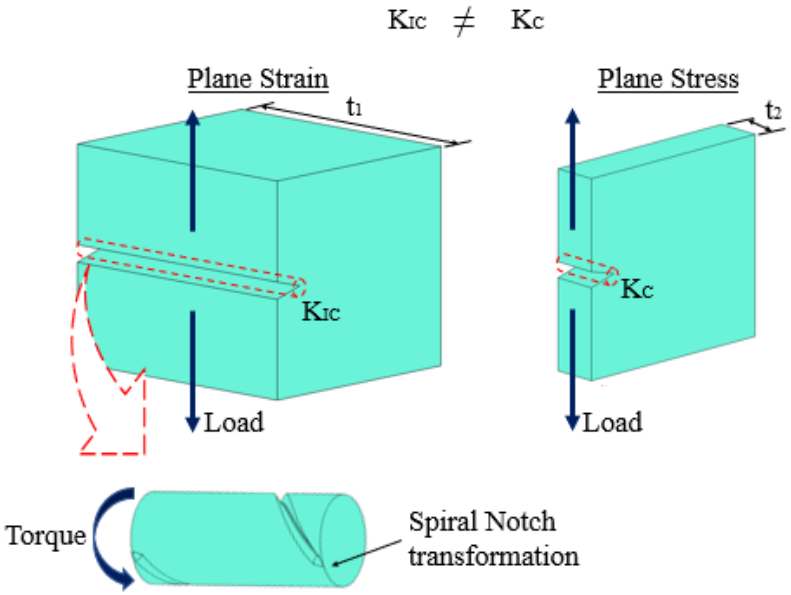

Figure 2. C(T) and SNTT specimen comparison and C(T) specimen size effect (Adapted from WANG, 2019).

According to Wang (2019), the specimen miniaturization is a fundamental goal of SNTT method. This is made possible because the K_{IC} values determined by the SNTT method are virtually independent of specimen size. By analyzing the stress and strain fields on the surface of C(T) specimen, it is noted that the information needed to determine the K_{IC} value manifests in a region very close to the crack tip. Therefore, when performing a test on an SNTT specimen, this region will extend along the entire notch, allowing the specimen miniaturization without the loss of validity of the K_{IC} value (Fig. 2).

Figure 3 shows the nominal dimension and geometry of an SNTT specimen with a 9.53 mm diameter. It is important to note that all the other dimensions were defined as a function of the specimen diameter, including the notch pitch. Additionally, it is noted the presence of a square section, which is responsible for passing the torque to the specimen.

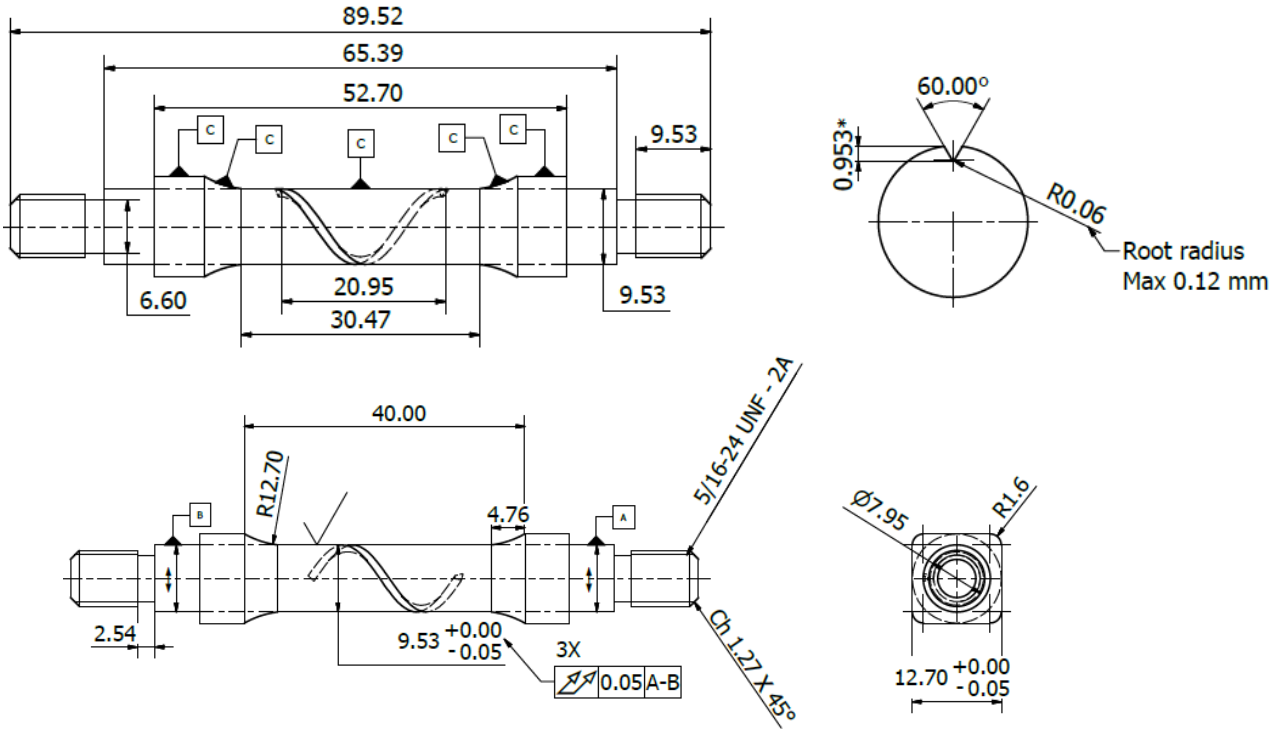

Figure 3. SNTT specimen with a diameter of 9.53 mm. All the dimensions are indicated in millimeters.

Wang (2019) obtained, by means of numerical simulations, equations to determine the material fracture toughness using the SNTT method. It was used finite elements performing energy release rates at different crack lengths with the respective torques and rotation angles. Figure 4 shows the evolution of the crack growth in the SNTT specimen with the finite elements' simulation, considering a specimen with a diameter (D) and a crack length (a). The ratio of the crack length over diameter varies from 0.1 to 0.45. Thus, it is important to mention that these equations are valid only for this range of a/D.

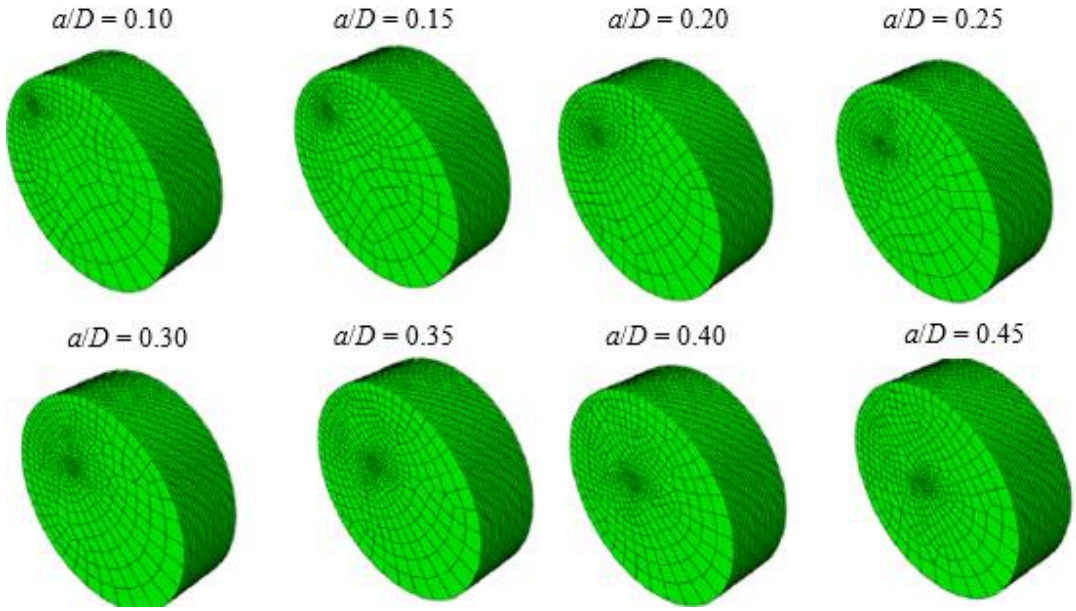

Figure 4. Evolution of crack growth in the SNTT specimen using the finite elements' simulation models (WANG, 2019).

The evolution of the SNTT compliance and the energy release rates were evaluated with the variation of the crack lengths. As a result, two non-dimensional parameters, the characteristic compliance, and the characteristic energy release rates of SNTT were obtained in order to quantify the crack growth during the SNTT process in different conditions and materials (Figs. 5 and 6). It can be noted that, regardless of the simulation conditions, the equations obtained were the same (WANG, 2019).

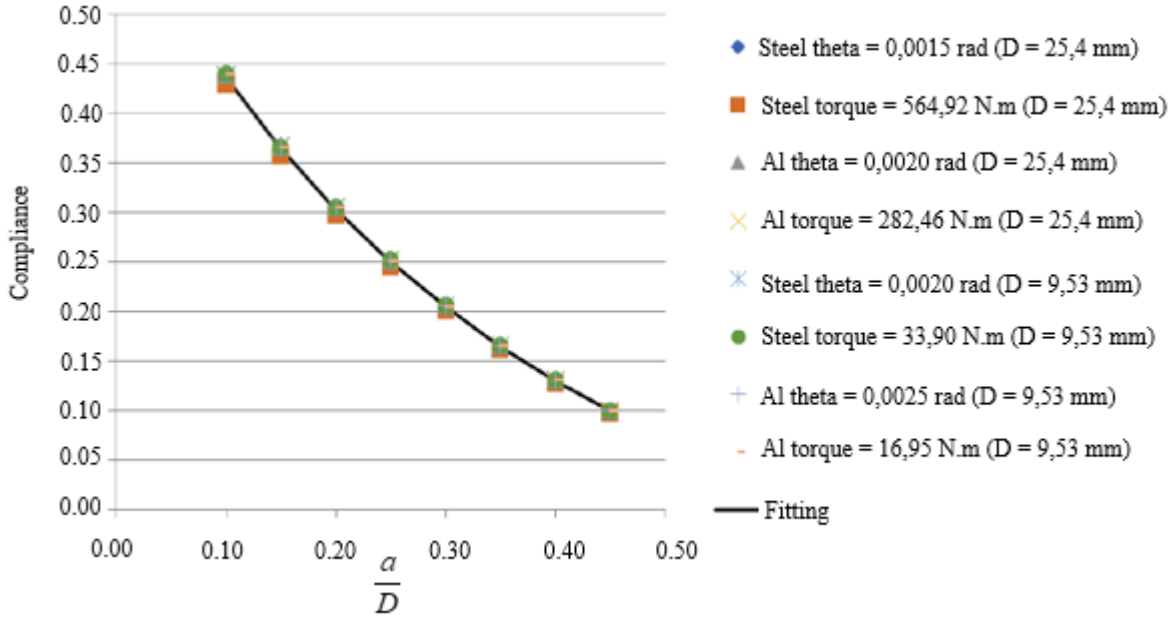

Figure 5. The scaled compliance evolution along the crack growth (WANG, 2019).

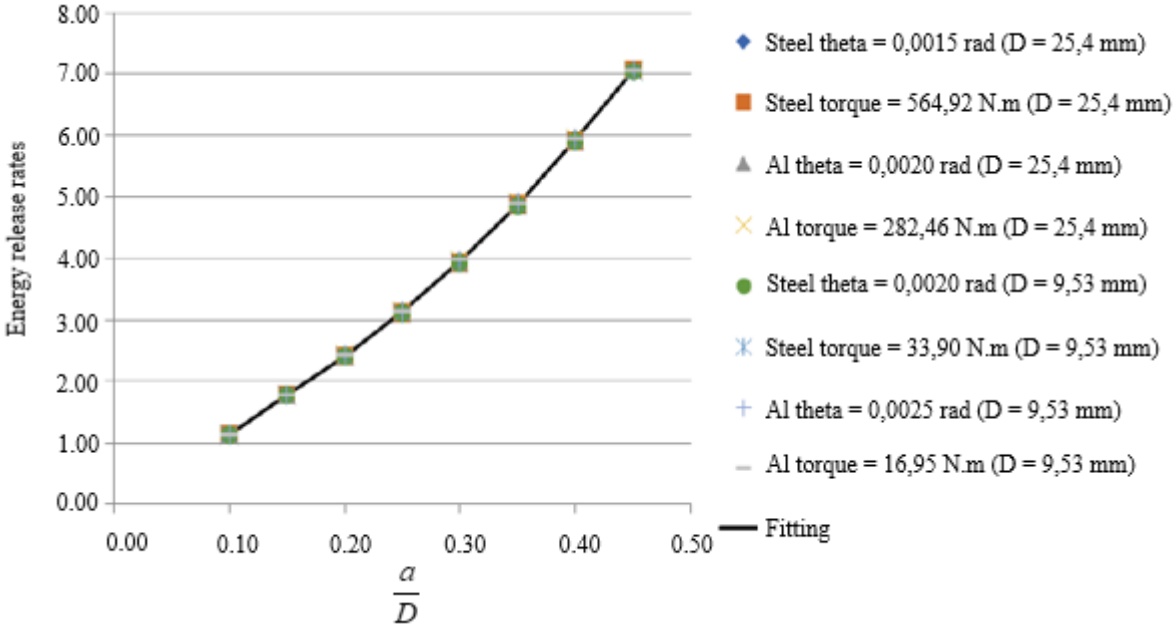

Figure 6. The scaled energy release rates evolution along with the crack growth (WANG, 2019).

Considering the important role of fracture toughness in predicting the material behavior and in preventing the occurrence of structural failure, it is inferred the need to obtain traceable toughness values. Metrological traceability requires, among other aspects, the measurement evaluation and declaration. According to Désenfant and Priel (2017), the measurement uncertainty declaration is as important as it is to report the measurement result itself. A measurement result without an assessment of its reliability is completely useless. The comparison between different measurements of the same measurand, as well as between a measurement result and a specification limit, are impossible to assess without knowing the uncertainty (BIPM et al., 2008). Thus, the present work aims to evaluate the measurement uncertainty associated with fracture toughness in SNTT tests. It is hoped to contribute to the traceability of results, as well as to comply with NBR ISO/IEC 17025 (2017).

2. METHODOLOGY

According to Wang et al. (2000), the value of the critical tension factor in the Mode I of loading (K_{IC}) can be estimated as given in Eq. (1).

$$K_{IC} = \sqrt{\frac{E \cdot G}{\left(1-\nu^2\right)}} \tag{1}$$

In Equation (1), E is the Young Modulus, ν is the Poisson ratio and G is the energy release rate that occurs during the test.

Wang et al. (2014) developed equations in order to evaluate the compliance evolution and the resistance of the specimen during the SNTT test. The Equation (2) makes possible to obtain the energy release rate G.

$$G = \frac{1}{A} T\theta \left(1-\frac{a}{D}\right)^2 \left[-154.56\left(\frac{a}{D}\right)^4 + 188.95\left(\frac{a}{D}\right)^3 - 62.398\left(\frac{a}{D}\right)^2 + 20.626\left(\frac{a}{D}\right) - 0.4716\right] \tag{2}$$

In Equation (2), A is the specimen cross-sectional area, a is the crack length observed after the failure, T is the torque, θ is the torsion angle and D is the specimen diameter.

From Equations (1) and (2) it is possible to notice that the fracture toughness is estimated as a function of seven input variables (A, a, D, T, θ, E and ν). Each of these variables depends on several factors, which contributes to the fracture toughness final uncertainty. Thus, uncertainty assessment is a difficult task. Therefore, in order to evaluate the uncertainty associated with fracture toughness and the energy release rate, the Monte Carlo method presented in the JCGM 101 (BIPM et al., 2008a) was applied, whereas for the others measurands (A, a, D, T, θ, E and ν) the GUM method, proposed in the JCGM 100 (BIPM et al., 2008b), was used.

During the calculation, the data concerning of specimen made of Inconel 718 with a 9.525 mm diameter were considered. For E and ν, the values presented by Souza (2018), 209.5 GPa and 0.3, respectively, were considered. Table (1) shows the measurement instruments used and the mathematical models proposed for the uncertainty assessment using the GUM method. It is important to mention that the uncertainties associated with the Young Modulus and Poisson coefficient were not estimated since their contribution to the final uncertainty should be minor. The mathematical model proposed for uncertainty assessment for the input variables A, a, D, T and θ are shown in Table 1.

Table 1. Measurement instruments and the mathematical models proposed for uncertainty assessment associated with input variables.

Variable – x	Measurement Instruments	Mathematical models
Torque	Torque transducer	$T = \bar{T} + \Delta R + \Delta C$
Torsion angle	Encoder	$\theta = \bar{\theta} + \Delta R + \Delta C$
Diameter	Micrometer for external measurements	$D = \bar{D} + \Delta R + \Delta C + \Delta EP$
Crack length	Optical microscope	$a = \bar{a} + \Delta R + \Delta C + \Delta AL$
Cross-section area	-----	$A = \frac{\pi D^2}{4}$

In the mathematical models of Tab. (1), $\bar{T}$, $\bar{\theta}$, $\bar{D}$ e $\bar{a}$ represent the variability associated with the average values obtained during measurements of each measurand, ΔR is the correction associated with the measurement system resolution, ΔC is the correction associated with the measurement system calibration, ΔEP is the correction associated with the parallelism deviation of the micrometer measurement faces and ΔAL is the correction associated with the microscope lens magnification. Figure 7 shows the main sources of uncertainties and their respective probability distribution considered during the assessment of the uncertainty associated with fracture toughness.

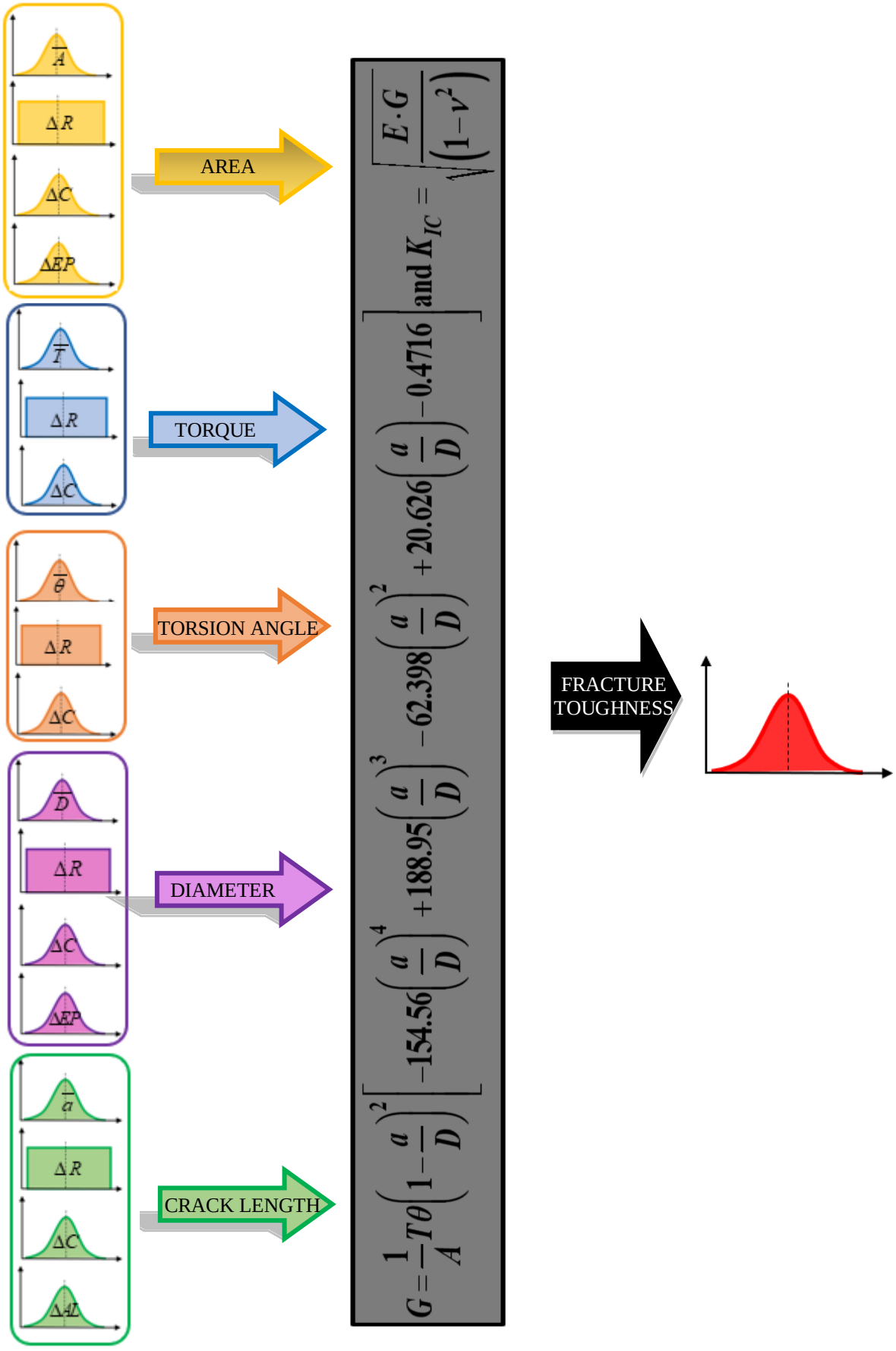

Figure 7. Schematic of the evaluation of uncertainty associated with the fracture toughness.

To determine the standard uncertainty associated with the variability average values, indicated by the: torque transducer, encoder, optical microscope and micrometer for external measurement, t-Student distributions were adopted, as indicated by Eq (3). The Equations (4) and (5) were used to determine the standard uncertainties associated with the measurement system resolution and calibration, respectively. To evaluate the standard uncertainty associated with the resolution, a rectangular distribution was adopted with infinite degrees of freedom.

$$u(\bar{x}) = \frac{s(x)}{\sqrt{n}} \tag{3}$$

$$u(\Delta R) = \frac{R(x)}{\sqrt{3}} \tag{4}$$

$$u(\Delta C) = \frac{U(C(x))}{k} \tag{5}$$

In Eqs. (3-5), *s(x)* is the experimental standard deviation of the measurements of each input variable; *n* is the number of the measuring cycles performed in each measurement; *R(x)* is the resolution of each measurement system; *U(C)* is the expanded uncertainty associated with the measurement system calibration and *k* is the correspondent coverage factor.

To determine the standard uncertainties associated with the parallelism deviation of the micrometer measurement faces and the correction associated with the microscope lens magnification was considered the information stated on the corresponding calibration certificate, as shown in Eqs. (6) and (7).

$$u(\Delta EP) = \frac{U(EP)}{k_{EP}} \tag{6}$$

$$u(AL) = \frac{U(AL)}{k_{AL}} \tag{7}$$

In Eqs. (6) and (7), *U(EP)* is the expanded uncertainty associated with the parallelism deviation of the micrometer measurement faces and k_{EP} is the correspondent coverage factor; *U(AL)* is the expanded uncertainty associated with microscope lens magnification and k_{AL} is the correspondent coverage factor.

Given the combined standard uncertainties of each input variables, the Monte Carlo method was applied in order to estimate the uncertainty associated with the *G* and, later, with the K_{IC}. The simulation was carried out using Microsoft Excel® 2019. In all cases, 1 000 000 iterations were performed. For both measurands, a histogram was constructed and the values of Skewness and Kurtosis were calculated. From the simulation results, it was possible to obtain the average and the standard deviation values associated with *G* and K_{IC}. Finally, considering the criterion established on JCGM 101 (BIPM, et al., 2008a) that defines that if Skewness and Kurtosis values are close of zero and three, respectively, it was possible to determine the value of the expanded uncertainty associated with each measurand as shown in Eq. (8).

$$U(y) = 2.00 \cdot s(y) \tag{8}$$

In Equation (8), $U(y)$ is the expanded uncertainty associated with the measurand and $s(y)$ is the standard deviation obtained by the simulated values.

3. RESULTS

Table (2) shows the combined standard uncertainty values (u_c (x)), the effective degrees of freedom (v_{ef}) and the coverage factor (k) obtained during the evaluation of the uncertainty associated with all input variables present in Eq. (1) and (2). It was possible to notice that the combined standard uncertainty values associated with the input variables with respect to their respective average values were low, with the highest value being 0.59 % for the crack length measurement.

Table 2. Combined standard uncertainties values, effective degrees freedom and coverage factor for input variables.

Input variable	u_c (x)	v_{ef}	k	Ratio u_c (x)/ Average value ($\bar{x}$)
Torque	0.278 (N.m)	4	2.78	0.28 %
Torsion angle	0.00006 (rad)	48	2.01	0.32 %
Diameter	0.013 (mm)	5	2.78	0.13 %
Crack length	0.017 (mm)	5	2.57	0.59 %
Cross section area	0.013 (mm²)	5	2.78	0.02 %

The values of Skewness and Kurtosis were 0.007 and 3.000 for *G*, respectively, whereas for K_{IC} these values assumed 0.013 and -3.002, respectively. Thus, the hypothesis of normality and symmetry of *G* and K_{IC} distribution could be confirmed. Figure 8 shows the distribution histogram of the *G* and the Fig. 9 of the K_{IC}, both obtained by Monte Carlo method.

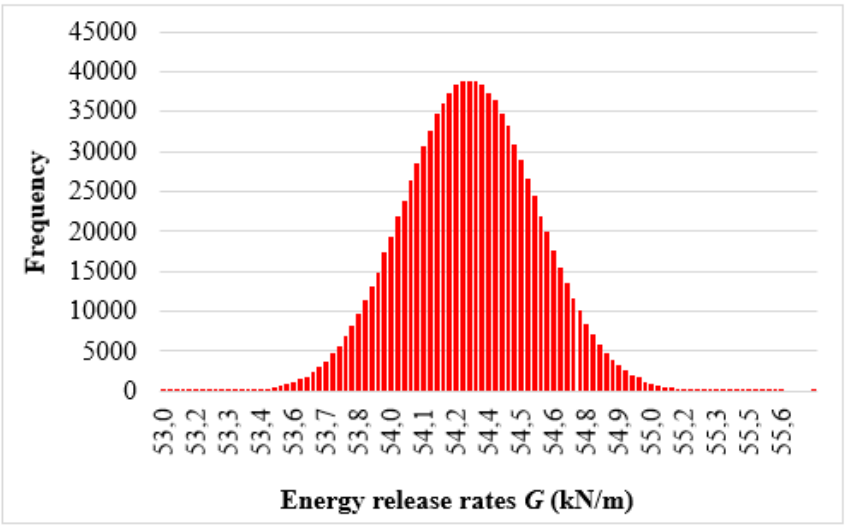

Figure 8. Normal distribution histograms of the values of *G* obtained by Monte Carlo method.

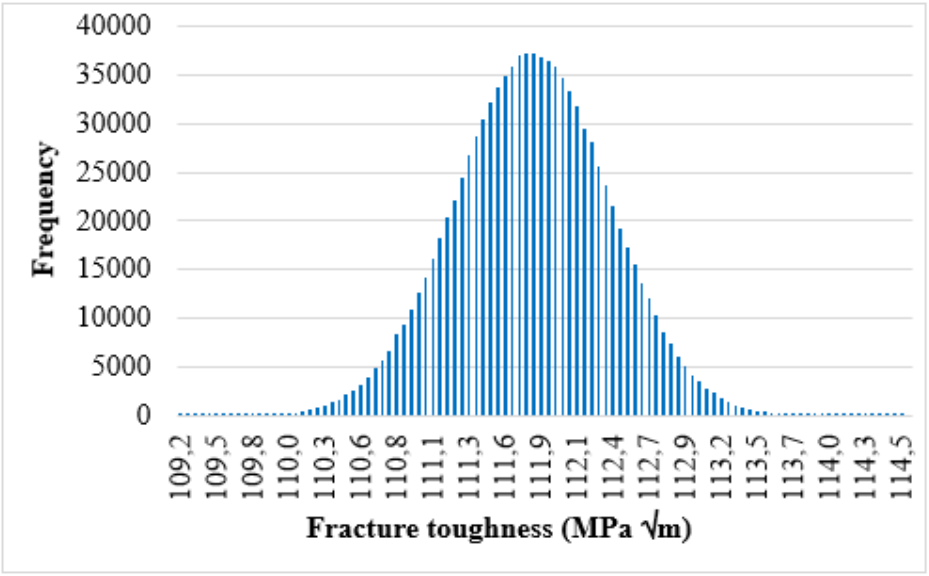

Figure 9. Normal distribution histograms of the values of K_{IC} obtained by Monte Carlo method.

The average value calculated for *G* by the Monte Carlo method was 54.280 kN.m^{-1} with an associated expanded uncertainty of ± 0.552 kN.m^{-1}. The result is satisfactory since these values represent 1.0 % the average value. On the

other hand, the value of K_{IC} was 111.787 $\text{MPa}\sqrt{\text{m}}$ with an expanded uncertainty of $\pm$ 1.137 $\text{MPa}\sqrt{\text{m}}$, representing 1.1 %.

Compared to the work of Sartori (2014), which obtained, by means of the CTOD method, the fracture toughness value for the Inconel 718 equal to 118 $\text{MPa}\sqrt{\text{m}}$, it can confirm that the fracture toughness estimation, by means of the SNTT method, has a similar and therefore satisfactory value. The difference between the results was approximately 5.3 %.

4. CONCLUSIONS

The results obtained for the fracture toughness were satisfactory and coherent, besides presenting a considerably low associated uncertainty, about 1.1 % in relation to the average value. Furthermore, it can be concluded that the present equation in the literature to model the energy release rate by simulated SNTT tests on finite elements was considered adequate to estimate the Inconel 718 fracture toughness value in this work, from considerations for the measurement instruments involved in the SNTT test.

5. ACKNOWLEDGMENTS

The authors acknowledge the CAPES, the CNPQ, the PETROBRAS and the LTAD for the financial and material support to carry out this work.

6. REFERENCES

ABNT NBR ISO/IEC 17025, 2017. *Requisitos gerais para competência de laboratórios de ensaio e calibração, Associação Brasileira de Normas Técnicas*. Rio de Janeiro: Associação Brasileira de Normas Técnicas. pp. 31, 2nd Edition.

ASTM E399-90, 2017. *Standard Test Method for Plane-Strain Fracture Toughness of Metallic Materials*. West Conshohocken: American Society for Testing Materials.

ASTM E740-88, 2001. *Standard Practice for Fracture Testing with Surface-Crack Tension Specimens*. West Conshohocken: American Society for Testing Materials.

ASTM E1820-01, 2001. *Standard Test Method for Measurement of Fracture Toughness*. West Conshohocken: American Society for Testing Materials.

BIPM (Bureau Internacional des Poids et Measures), 2008a. *JCGM 100: Evaluation of Measurement Data – Guide to the Expression of Uncertainty in Measurement.* Geneva Switzerland, 134 p.

BIPM (Bureau Internacional des Poids et Measures), 2008b. *JCGM 101: Evaluation of measurement data - Supplement 1 to the "Guide to the Expression of Uncertainty in Measurement" - Propagation of distributions using a Monte Carlo method.* Geneva Switzerland, 90 p.

Désenfant, M.; Priel, M.; 2017. "Reference and additional methods for measurement uncertainty evaluation", Measurement. 95 339–344. doi:10.1016/j.measurement.2016.10.022.

Sartori, M., 2014. *Avaliação da tenacidade à fratura da liga Inconel 718 sob proteção catódica em água do mar sintética utilizando a técnica step loading.* Dissertação de Mestrado, Universidade Federal do Rio Grande do Sul, Porto Alegre, Brasil.

Souza, D. E. F. 2018. *Efeito dos tratamentos térmicos e da severidade do entalhe na susceptibilidade à fragilização por hidrogênio do Inconel 718, avaliada pelo método de RSL*. Dissertação de Mestrado, Universidade Federal de Uberlândia, Uberlândia, Brasil.

Wang, J. A.; Liu K. C.; McCabe, D. E; 2000. "Using torsional bar testing to determine fracture toughness". *Fatigue & Fracture of Engineering Materials & Structures*, Vol. 23, No.11, pp. 917-927.

Wang, J. A.; Liu K. C.; McCabe, D. E; 2004. "A New Approach to Evaluate Fracture Toughness of Structural Materials". *Journal of Pressure Vessel Technology*, Vol. 126, No 4, pp. 534-540.

Wang, J. A.; Liu K. C.; McCabe, D. E; 2002. "An Innovative Technique for Measuring Fracture Toughness of Metallic and Ceramic Materials", *Fatigue and Fracture Mechanics*: *33rd Volume*, W. G. Renter and R. S. Piascik, Eds., ASTM International, West Conshohocken, PA.

Wang, J. A., Ren, F.; Tin, T. Liu, K. C., 2014. "The development of in situ fracture toughness evaluation techniques in hydrogen environment", *International Journal of Hydrogen Energy*. Vol. 40, No 4, pp. 2013-2024.

Wang, J. A.; 2019. “Fracture Toughness Evaluation for Sandia Mock-up Stainless Steel Canister Weldment Using Spiral Notch Torsion Fracture Toughness Test”, *Materials Science & Technology Division.* Oak Ridge National Laboratory, Oak Ridge, Tennessee, United States of America.

7. RESPONSIBILITY NOTICE

The authors are the only responsible for the printed material included in this paper.